Magnetic-field-modulated written bits in TbFeCo thin films: Transmission electron microscopy Lorentz and scanning electron microscopy with polarization analysis studies

M. Aeschlimann,[a] M. Scheinfein, and J. Unguris
National Institute of Standards and Technology, Gaithersburg, Maryland 20899

F. J. A. M. Greidanus[b]
Philips Research Laboratories, P.O. Box 80.000, 5600 JA, Eindhoven, The Netherlands

S. Klahn
Philips GmbH Forschungslaboratorium Hamburg, D-2000 Hamburg, Federal Republic of Germany

(Received 29 May 1990; accepted for publication 3 July 1990)

Domains written thermomagnetically in TbFeCo thin films are studied with Lorentz transmission electron microscopy (TEM) and scanning electron microscopy with polarization analysis (SEMPA). Four different rare-earth/transition-metal compositions $Tb_xFe_yCo_{1-x-y}$ are examined. The domain structures observed with both techniques are similar even though TEM Lorentz only detects the transverse component of the net magnetic field along the electron's trajectory through the sample, while SEMPA detects the surface electron-spin polarization (magnetization). We find that the magnetic contrast in the SEMPA measurements is proportional to the magnetization of the transition-metal (TM) subnetwork which is antiferromagnetically coupled to the rare-earth (RE) subnetwork. This allows high-contrast SEMPA images to be acquired even when the system is magnetically compensated ($M_s = |M_{RE} - M_{TM}| = 0$). The surface magnetization can be explained by assuming that the surface of the TbFeCo alloy consists of an outermost thin oxide layer followed by an Fe-rich subsurface layer. The importance of the demagnetizing field on the switching and domain nucleation process for thermomagnetically written bits is examined.

I. INTRODUCTION

Direct overwrite magneto-optical (MO) disk technology has recently been the target of extensive research.[1,2] One of the most promising overwriting techniques is magnetic-field modulation (MFM).[3,4] With this method the MO layer is heated with a continuous laser beam while applying a magnetic field, whose direction is switched at high frequency. The magnetic field is frequency modulated in accordance with the information to be stored such that characteristic crescent-shaped domains with variable length remain in the magneto-optical film. The size and shape of the domains will ultimately effect the packing density of the magneto-optical medium. Any irregularities in the domain shapes or sizes could introduce noise into the media. In order to understand the magnetic domain formation in magneto-optical materials, it is extremely helpful to obtain clear images of the magnetic microstructure.

Thermomagnetically written bits are read optically by measuring the Kerr rotation or ellipticity of the reflected polarized light. Kerr microscopy is therefore well suited for the observation of written bits in MO materials, and observations can be made without removing any of the passivation layers.[5] However, the lateral spatial resolution of this microscopy is diffraction limited to approximately 0.4 μm at optical wavelengths.

Electron microscopy can be used to observe magnetic microstructure with higher spatial resolution. Lorentz transmission electron microscopy (TEM) has been used successfully to obtain high-resolution (< 100 nm) images of MO materials with high net magnetizations such as $Tb_{19}Fe_{81}$ or $Tb_{32}Fe_{68}$.[6,7] TEM Lorentz contrast is very weak, however, for intermediate compositions (23%–27% Tb), which have compensation temperatures (T_{comp}) near room temperature. This is due to the small magnetic fields which result from the small net magnetization M_s for temperatures near T_{comp}. Furthermore, techniques utilizing transmission electron microscopy require thin films which must be floated off an initial deposition substrate or prepared on silicon thin-film windows.[8]

In scanning electron microscopy with polarization analysis (SEMPA), a focused beam of high-energy electrons is rastered point by point across the sample surface. The polarized secondary electrons emitted from the sample surface, which retain the spin-polarization orientation characteristic of the local region of the sample being probed, are spin analyzed.[9] The lateral spatial resolution of this technique is ultimately limited by the final electron probe size formed by the long focal length objective in SEM. In our implementation, a nominal lateral spatial resolution of 70 nm is attainable. The spin-polarized electrons excited in SEMPA are the result of the electron cascade which creates electron-hole pairs in the material. We will show that most of the *polarized* secondary electrons in rare-earth/transition-metal alloys originate from the transition metal. SEMPA, which analyzes all three spin components of the emitted secondary electrons created

[a] Present address: Center for Photoinduced Charge Transfer, Department of Chemistry, University of Rochester, Rochester, NY 14627.
[b] Present address: Philips Laboratories, 345 Scarborough Road, Briarcliff Manor, NY 10510.

near the surface, has an estimated probing depth on the order of a few nm.[10,11] Due to the surface sensitivity of this technique an ultrahigh vacuum environment is required, and any passivation layer must be removed by ion sputtering prior to analysis. The MO materials examined here have surface segregation regions with properties which are significantly different from those in the bulk. SEMPA is thus an ideal technique to investigate these surface regions.

Thermomagnetically written bits in a TbFeCo alloy have also been observed by magnetic force microscopy.[12] The magnetic contrast of this technique is achieved as a result of the magnetostatic interaction between a magnetic tip and the fringe fields of a magnetic sample. A lateral spatial resolution in the magnetic image of 25 nm is achieved. This technique is nondestructive and the passivation layer need not be removed prior to observation. However, the observed contrast is a complex convolution of the tip/sample magnetostatic interaction and can be difficult to interpret. Since the signal depends on the magnetic induction as in TEM Lorentz, the contrast is also weak when sample temperatures are near T_{comp}.

We have used both TEM Lorentz and SEMPA to image thermomagnetically written bits in MO materials. The ability to investigate the sample with both techniques is quite powerful because the two methods for observation of magnetic microstructure complement each other. TEM Lorentz is sensitive to the integrated magnetic structure throughout the bulk, while SEMPA images the surface magnetic structure. In addition, the magnitude and direction of the surface magnetization orientation can be quantitatively analyzed using SEMPA. Surface segregation in these MO materials may be of great importance in understanding the nucleation and switching of thermomagnetically written domains. The surface regions may also contribute to the intrinsic noise in the readback process for MO media. We compared data from different compositions of $Tb_xFe_yCo_{1-x-y}$ at different applied magnetic fields. We are able to show the strong influence of the demagnetizing field from the neighboring region which acts on the area between the Curie radius and the coercive radius.[13] This is the region in which nucleation and domain growth occur during the thermomagnetic writing process.

II. SAMPLE PREPARATION AND CHARACTERIZATION

A series of four different $Tb_xFe_yCo_{1-x-y}$ films were fabricated. The composition of the four films are summarized in Table I. The films were nominally 45 nm thick, and were prepared by three-gun electron-beam evaporation. The films were deposited onto specially prepared silicon wafers which have a 10-nm-thick Si_3N_4 overlayer. For observation in TEM Lorentz, the wafers were back etched revealing a square Si_3N_4 thin-film window. The preparation of such structures has been described by Jacobs and Verhoeven.[8] The MO layer was protected against corrosion and oxidation by a 10-nm aluminum layer and a 25-nm SiO_2 overlayer.

TABLE I. Composition and properties of the MO materials.

Sample	Composition	T_c (K)	T_{comp} (K)
1	$Tb_{30}Fe_{62.5}Co_{7.5}$	450	$> T_c$
2	$Tb_{27.2}Fe_{65.5}Co_{7.3}$	461	310
3	$Tb_{23.6}Fe_{67.6}Co_{8.8}$	473	214
4	$Tb_{21.2}Fe_{71.9}Co_{6.9}$	473	$\leqslant 0$

The temperature dependence of the coercive field H_c was obtained from Kerr hysteresis curves, and is shown in Fig. 1. The temperature dependence of the saturation magnetization M_s was determined from torque measurements,[14] and is shown in Fig. 2. The quality factor $Q = K_u/2\pi M_s^2$, where K_u is the bulk magnetocrystalline anisotropy, is greater than 1 at all temperatures for all samples studied. This indicates that the bulk magnetization of the domains is perpendicular to the film surface ($T < T_c$). No bulk in-plane magnetization was observed.

The magnetic domains were recorded on the Si wafer disk using a standard optical recorder. Since there are no pregrooves on the wafer surface, the recorder was adjusted for air-incident operation in the "free-running" mode. First, the whole thin-film window was heated with the laser and magnetized uniformly in the positive direction. The positive direction has the film normal pointing out of the page and towards the viewer in the images to be presented. Different tracks were then written by accurate mechanical positioning of the lens. The high-frequency MFM fields were generated by a specially designed head[15] operating at a distance of 0.5 mm above the MO layer surface.

The films were observed first by TEM Lorentz using a Philips EM 301 electron microscope operated at 100 keV. In order to avoid the deleterious effects of stray fields, the objective lens was switched off. The imaging was done using the diffraction lens only. In materials with perpendicular anisotropy, it is in principle possible to image the components of the field (magnetization) perpendicular to the beam in the domain walls. However, the wall thicknesses for these materials are only about 10 nm due to the extremely large anisotropy. Thus it is extremely difficult to measure the structure in the domain walls. When the sample is tilted

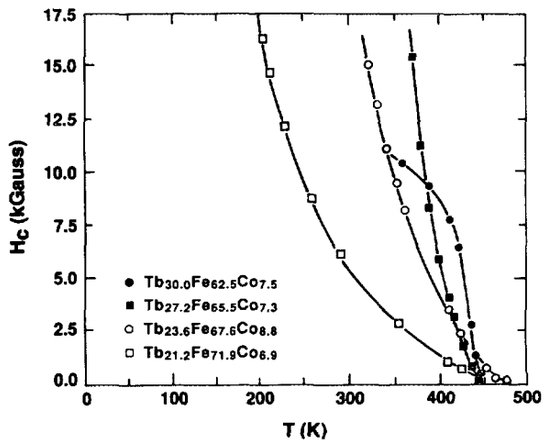

FIG. 1. Coercive field H_c, as a function of temperature for the four MO alloys.

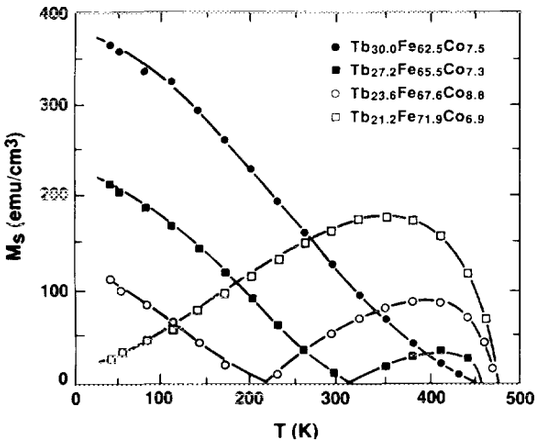

FIG. 2. Saturation magnetization M_s as a function of temperature for the four MO alloys.

there are oppositely oriented components of the net magnetization, perpendicular to the electron beam, on either side of a domain wall.[16] In this way, domain walls are imaged, but contrast is only obtained on the screen if the image plane is sufficiently far removed from the specimen (Fresnel contrast).

After TEM Lorentz observation, the samples were introduced into the UHV system for SEMPA observation. The passivation layer on the films was removed by sputtering with a 2-keV Ar^+-ion beam while monitoring the composition by Auger electron spectroscopy (AES). After this cleaning process, the samples were observed with SEMPA. A complete description of the SEMPA apparatus has been given elsewhere.[9,17]

III. DOMAIN OBSERVATION

Micrographs obtained by TEM Lorentz for the four different sample compositions (1–4) of Table I are shown in Figs. 3(a)–3(d), respectively. All of the thermomagnetically written bits were formed using identical laser power of 6.2 mW (dc). The domains in the vertical columns in Fig. 3 correspond to MFM written bits with different applied fields. Starting in each figure at the left and moving to the right, the first column contains three or four marker bits and, in the successive columns, the field strength used to write the MFM bits is 0, 80, 120, 200, 300, and 400 Oe, respectively. The image contrast is weakest for samples 2 and 3 in Figs. 3(b) and 3(c) due to the low net magnetization of these films near room temperature (see Fig. 2). The domains in sample 1 in Fig. 3(a) show a complex and irregular shape when compared to the other three samples. This indicates that the domain formation in this sample may procede by a different mechanism than in the other samples. Characteristic crescent-shaped domains are visible in Figs. 3(b)–3(d). Small subdomains (typically 0.1–0.3 μm) are observed within the MFM written domains for low-field intensity in the Fe-rich films [Figs. 3(c) and 3(d)]. In Fig. 3(d), the second column from the left (written in zero magnetic field) is totally demagnetized by this subdomain formation, hence no crescent-shaped domains are formed. A discussion of domain formation in these MO films will follow later.

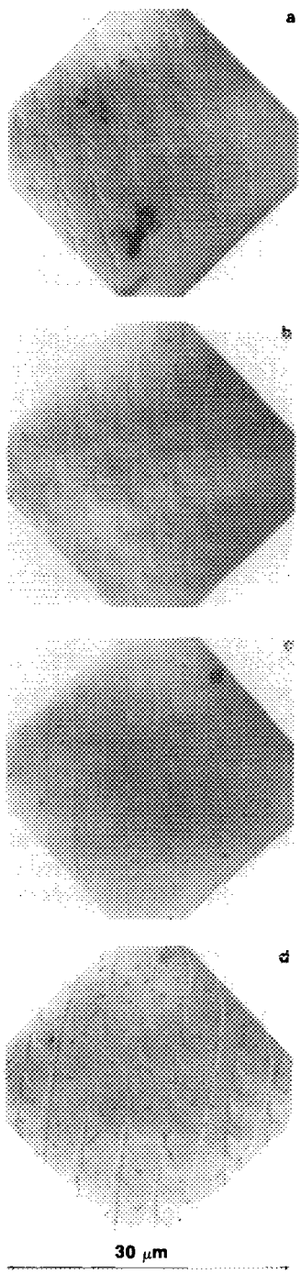

FIG. 3. TEM Lorentz images for (a) sample 1 ($Tb_{30}Fe_{62.5}Co_{7.5}$), (b) sample 2 ($Tb_{27.2}Fe_{65.5}Co_{7.3}$), (c) sample 3 ($Tb_{23.6}Fe_{67.6}Co_{8.8}$), and (d) sample 4 ($Tb_{21.2}Fe_{71.9}Co_{6.9}$). Each image has domains written in vertical tracks where each track utilizes a different applied magnetic switching field. Starting at the left and moving to the right, the first column contains three or four marker bits and then the switching field intensities are 0, 80, 120, 200, 300, and 400 Oe.

SEMPA domain images are shown in Figs. 4(a)–4(l) for identical samples cut from the same wafer. Each image in Fig. 4 is 30 μm on a side. Each horizontal row in Fig. 4

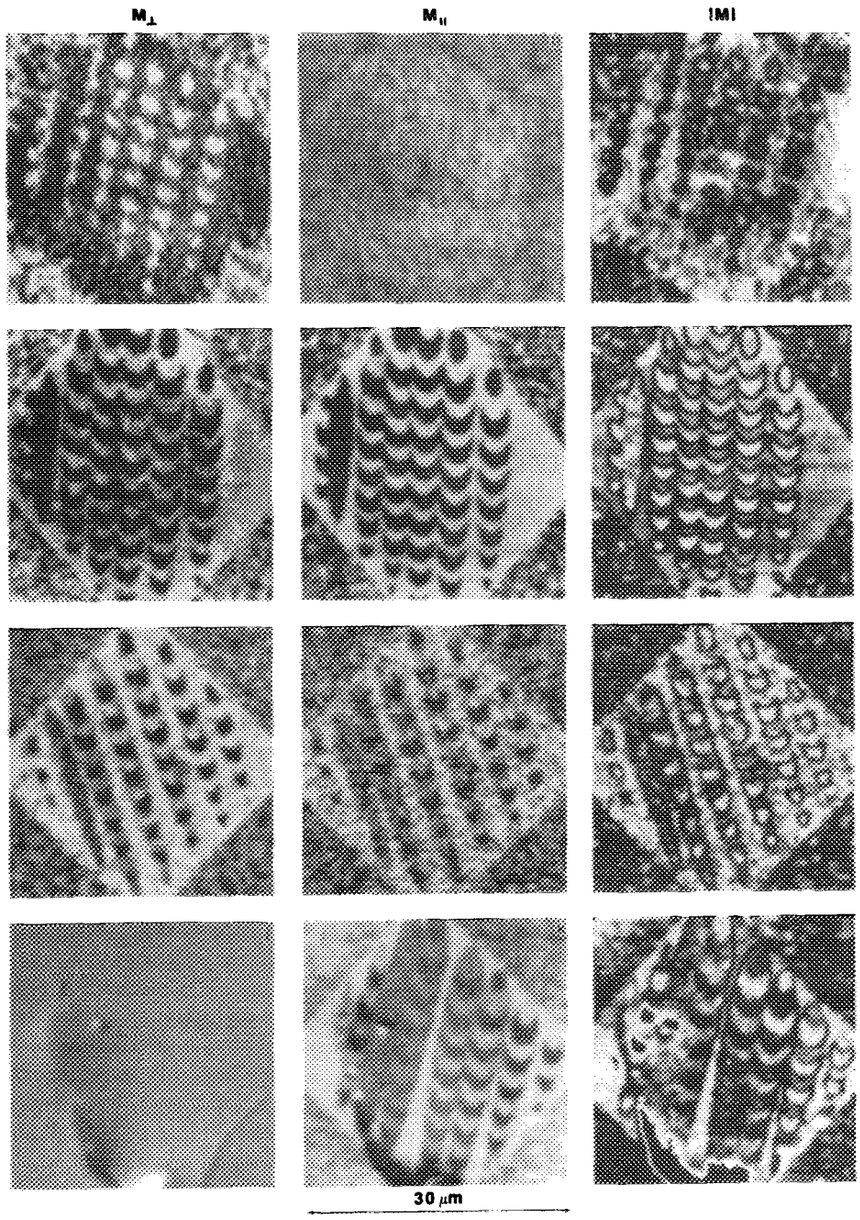

FIG. 4. SEMPA images from the four MO alloys. Moving left to right, the vertical columns of images are the out-of-plane ($M_\perp$), in-plane ($M_\parallel$), and magnitude ($|M|$) of the transition-metal magnetization. The images are 30 μm across. The horizontal columns are for sample 1 (30% Tb), sample 2 (27.2% Tb), sample 3 (23.6% Tb), and sample 4 (21.2% Tb) beginning at the top and moving down.

consists of SEMPA images from a different sample. The first horizontal row is from sample 1, the second row from sample 2, and so on. Moving left to right across the figure, the vertical columns contain SEMPA images of the out-of-plane magnetization component, $M_\perp$, the in-plane magnetization component, $M_\parallel$, and the magnitude of the magnetization, $|M|$. In the first two columns, the gray scale indicates the magnitude of the polarization vector measured along the specified direction. White (black) indicates a polarization in the negative (positive) direction. Since the magnetic moment of the electron is negative for positive spin ($\mu < 0$), white (black) indicates a magnetization in the positive (negative) direction. We conclude below that the secondary electron spin polarization is dominated by the 3*d* electrons of the transition metals Fe and Co and hence the magnetization that we observe in the image is that of the transition-metal subnetwork.

When the in-plane and out-of-plane magnetization images are added in quadrature pixel by pixel, the magnitude of the magnetization, $|M| = \sqrt{M_\parallel^2 + M_\perp^2}$, as shown in the third column of Fig. 4, results. In all of these magnitude images white indicates high magnetization and black is zero. The black outline around the written bits is a consequence of the probe radius being larger than the domain-wall width. This instrumental artifact results from averaging the magnetization across a domain wall, and causes some loss in the magnitude of the polarization signal at the wall.[17] With the exception of the wall region, the magnitude of the magnetization within a domain should be uniform. However, when switching is incomplete, numerous small subdomains

(smaller than the probe radius) are formed, and we expect the magnitude of the average magnetization within the probe radius to be diminished. In this way we will use the magnitude images in Fig. 4 as a measure of how complete the domain switching was in the overwrite process. For example, in Fig. 4(f), the domains written with different field strengths possess the same magnitude of the magnetization, and thus the overwrite process completely switched the domain orientation.

The magnitude of the magnetic contrast in SEMPA is a function of the Tb concentration in the MO alloys. Specifically, as the polarized secondary electrons originate very near the surface, the magnetic contrast observed in SEMPA will depend on the chemical composition and stoichiometry of the near-surface region. The relative magnitude of the polarization for secondary electrons from these MO alloys is plotted in Fig. 5 as a function of the bulk Tb concentration. We emphasize that the near-surface Tb concentration may differ from that in bulk. We observe that the polarization (magnetization) signal rises monotonically as the Tb concentration decreases in the bulk. Since the polarized secondary electrons originate predominately from the transition-metal subnetwork, as the bulk Fe and Co concentration increases, so does the magnetic contrast observed with SEMPA. The magnetic contrast in SEMPA does not depend specifically on the net magnetization of this ferrimagnetic system, as it does in TEM Lorentz.

The source of the magnetic contrast in the SEMPA images can also be understood by examining the out-of-plane component of the magnetization from sample 1 in Fig. 4(a). With a Tb atomic concentration of 30%, there is no temperature at which compensation occurs below the Curie temperature (see Table I). This means that the net magnetization is dominated by the Tb subnetwork for all temperatures. As described previously, first the whole thin-film window was heated by the laser and written uniformly such that the magnetization was directed in the (positive) out-of-plane direction. Thus, the rare-earth (Tb) subnetwork of the background magnetization within the square window is oriented along the surface normal and the transition-metal subnetwork (Fe,Co) must be oriented antiparallel to the surface normal. The SEMPA image of Fig. 4(a) shows that the background magnetization in the thin-film window is negative. Since the transition-metal (Fe,Co) subnetwork magnetization has its moment oriented antiparallel to the surface normal, the polarized secondary electrons must originate predominately from the transition-metal (Fe,Co) subnetwork. This is also consistent with the domain image observed for sample 2 [Fig. 4(d)] which has a compensation temperature of 310 K. In this case, the Tb subnetwork also dominates the net magnetization at room temperature. However, the background magnetization of Fig. 4(d) is in the positive direction (white), oppositely oriented to that in Fig. 4(a). This results because the magnetization orientation of the background, within the square, is determined by the subnetwork which dominates the magnetization at the writing temperature T_{coerc}.[13] In sample 2, $T_{\text{coerc}} \sim 450K > T_{\text{comp}}$. Thus at the writing temperature, the transition-metal subnetwork is oriented parallel to the applied field. During the cooling process, the orientation of the written domain is frozen in due to the high coercivity, independent of whether or not the compensation temperature is above [Fig. 4(d)] or below [Fig. 4(g)] room temperature. Accordingly, the background magnetization for the transition-metal subnetwork is also parallel to the applied field at the observation temperature, and appears as white in the SEMPA M images. Only at compensation temperatures above the Curie temperature, as in sample 1, is the Tb subnetwork dominant at the writing temperature [black background; see Fig. 4(a)].

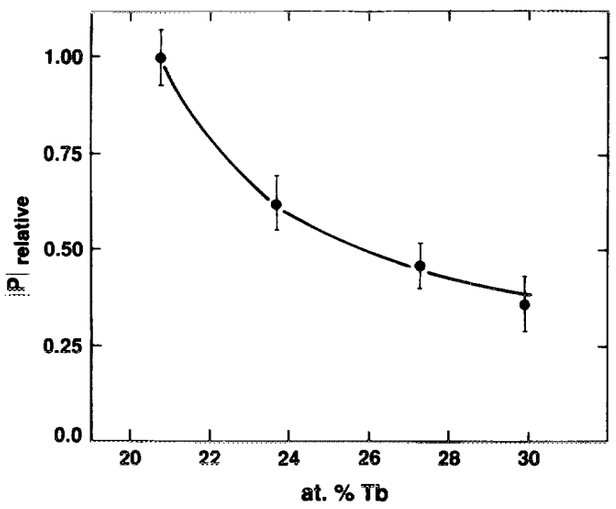

FIG. 5. Relative polarization measured in SEMPA for the TbFeCo alloys as a function of the bulk Tb atomic concentration.

This is the first observation of a ferrimagnetic system using SEMPA, and the first demonstration that the polarized secondary-electron cascade, which underlies the magnetic contrast in SEMPA, is dominated by the $3d$ valence electrons from the transition metals in these alloys.

Now we can analyze the SEMPA images of Fig. 4, and compare them to the TEM Lorentz images of Fig. 3. The domain structure, as a function of the applied magnetic field, is also observed for the individual vertical columns in each of the 12 images which comprise Fig. 4. No in-plane components of the magnetization were found in sample 1 (30% Tb) as evidenced by the lack of magnetic contrast in Fig. 4(b). Almost crescent-shaped domains are formed only for large switching fields ($H_{\text{app}} > 200$ Oe). The domain structure becomes quite irregular for smaller applied fields. The domain shapes are duplicated in both the TEM Lorentz and SEMPA images of sample 1, although the associated edge irregularities are more pronounced in the TEM Lorentz images.

The domain images of sample 2 (27.3% Tb) as observed with SEMPA and TEM Lorentz are also similar. SEMPA reveals that a much more complicated domain structure is present at the surface. There is an out-of-plane component of the magnetization shown in Fig. 4(d) and an in-plane component of the magnetization shown in Fig. 4(e). The (surface) magnetization is no longer completely normal to the

surface. A discussion of this surface in-plane magnetization layer at lower Tb concentrations will follow in the next section. The image of the magnitude of the magnetization of sample 2 [Fig. 4(f)] indicates that for all switching fields ($H_{app} > 0$) the magnetization maintains a nearly constant value within the written domains. No subdomains are formed within the written domains. Notice that without any applied field [Fig. 4(e), second column from the left] only domains oriented in a direction opposite to the background can be written in the MFM-mode.

In Figs. 4(g)–4(i), SEMPA images for the out-of-plane, in-plane, and magnitude of the magnetization from sample 3 (23.6% Tb) are shown. The in-plane and out-of-plane magnetization components are nearly equal, demonstrating that the magnetization points out of the surface at 45°. In the leftmost columns of the magnitude image [Fig. 4(i)], the magnitude of the magnetization within the written domains is less than that in the background, indicating that these domains are not entirely overwritten. The domains at the right side of the image, written at higher fields, do not exhibit subdomain formation since they appear to have the same magnitude of magnetization as the background.

Finally, the SEMPA images of sample 4 (21.2% Tb) are given in Figs. 4(j)–4(l). The lack of out-of-plane magnetization is evidenced in Fig. 4(j). The entire surface magnetization lies in-plane, as shown in Fig. 4(k). Nevertheless, these in-plane domain structures are similar to the (perpendicular) bulk domain shapes observed with TEM Lorentz. The structure at the bottom of Figs. 4(j)–4(l) is a topographic defect which penetrates into the thin film window. Figure 4(l) illustrates once again that for lower switching fields (the left four columns in the figure) the magnitude of the average magnetization within the probe radius is decreased, resulting from incomplete switching during the overwrite process. In this very iron-rich composition, the domains are only well formed when the switching field strength is large.

Higher-resolution SEMPA images at the largest applied fields (300 and 400 Oe) from samples 1–4, respectively, are shown in Figs. 6(a)–6(d). All images show the out-of-plane component of the magnetization except for sample 4 [Fig. 6(d)] which shows the in-plane magnetization. These images are 7.2 μm on a side. The domain boundaries are well resolved, indicating that the lateral spatial resolution in the images is about 100 nm. Notice also that the SEMPA images display high contrast even when the sample is nearly magnetically compensated ($M_s \sim 0$) such as in sample 2 [Fig. 6(b)]. The variation in the written domain width at different compositions are due to variations in the intrinsic magnetic parameters such as the temperature dependence of the coercivity and magnetization. The thickness variation of the protective metallic Al overlayer on different samples also affects the written domain width.

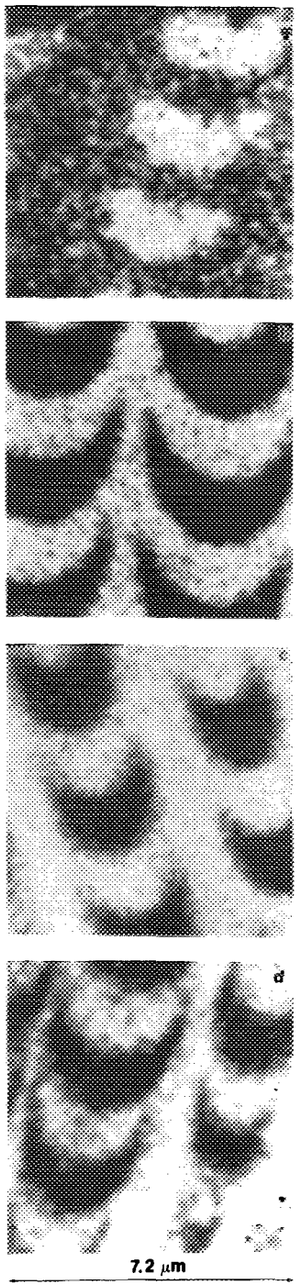

FIG. 6. High magnification SEMPA images, 7.2 μm across. (a) $M_\perp$ from sample 1 (30% Tb), (b) $M_\perp$ from sample 2 (27.2% Tb), (c) $M_\perp$ from sample 3 (23.6% Tb), and (d) $M_\parallel$ from sample 4 (21.2% Tb).

IV. IN-PLANE MAGNETIZATION AT SURFACES

It is known that the surface segregation and oxidation of the rare-earth elements in transition-metal rare-earth alloys produces a variation in the magnetic behavior near the surface.[18,19] Using spin-polarized photoemission on TbFe films, Aeschlimann *et al.*[20,21] have shown that an in-plane magnetic layer can be present at the near surface. They show that segregation and oxidation of the rare-earth Tb results in a nonmagnetic Tb-Fe-oxide surface layer, which is followed by an Fe-rich subsurface layer and finally the bulk material (three-layer model).[20,21] The Fe-rich subsurface layer exhibits a lower perpendicular anisotropy K_U and larger saturation magnetization M_s than the bulk alloy. This is due to

the depletion of the rare-earth compensating magnetic moments. Decreasing the anisotropy K_U (normal to the surface) and increasing the saturation magnetization M_s both cause preferentially in-plane oriented magnetization at surfaces. We will show that qualitative observations made with SEMPA are in agreement with this simple model. The Tb concentration appears to have a direct effect on the orientation of the surface magnetization. In Fig. 7, a possible representation of the surface magnetic structure in TbFeCo alloy thin films is shown. The diagrams correspond from left to the right: sample 1 (30% Tb) which has the surface magnetization oriented normal to surface; sample 3 (23.6% Tb) which has the surface magnetization at 45° to the surface; and sample 4 (21.2% Tb) which has the surface magnetization parallel to the surface. In the case of rare-earth-rich films, such as sample 1 (30% Tb), no in-plane magnetization was observed. This indicates that the in-plane layer, if it exists at all, must be thinner than the probing depth of SEMPA for magnetic microstructure observation. For low Tb concentration films, such as sample 4 (21.2% Tb), no out-of-plane magnetization was observed. However, this in-plane subsurface layer is not completely decoupled from the bulk. The subsurface layer seems to have a preferential easy in-plane direction. The reason for this (uniaxial) in-plane anisotropy in these amorphous alloys could be the result of non-normal evaporation angles during film growth. Nevertheless, the surface domains are similar to the bulk domains imaged by TEM Lorentz [see Figs. 3(d) and 4(k)]. This indicates that the subsurface region must be thick enough to allow a complete 90° rotation of the magnetization from the perpendicular orientation in the bulk to the in-plane orientation in the last magnetic layers of the subsurface [see Fig. 7(c)]. For intermediate alloys such as sample 3, the rotation is incomplete and hence the measured orientation is neither perfectly into or out of the plane of the surface as shown in Figs. 4(g) and 4(h).

We conclude that the migration and oxidation of the rare earth occurs immediately after film growth or after sputtering away the protective overlayers of Al and SiO_2 because we observe that the surface magnetic properties stays constant for few days in UHV. This is in full agreement with spin-polarized photoemission data.[20] It should be noted that this fast segregation process may not only be an undesirable effect which occurs on removal of the protective overlayer. The same process can also occur during the period of time between finishing the TbFeCo-alloy film evaporation and starting the deposition of the protective layer. During this period, the fresh TbFeCo-alloy film is exposed to background impurities in the preparation chamber, which is normally operated at a much higher background pressure than our UHV system ($P_{\mathrm{SEMPA}} = 5\times 10^{-10}$ Torr).

In Fig. 8, we summarize our results by showing the orientation of the nucleated domains for three different alloys switched by the indicated external fields. For an externally applied field $\mathbf{H}_{\mathrm{app}}$, oriented normal to the film surface, the subsystem (either transition metal or Tb) which is aligned parallel to the field depends upon which subnetwork has the larger magnetic moment for that particular alloy composition at the writing temperature. In all samples the bulk magnetization points along the field direction. Only sample 1 (30% Tb) has the Tb moment aligned with the field, and the Fe and Co moments aligned antiparallel to the field. As SEMPA is sensitive primarily to the polarized secondary electrons originating in the transition metals, we include the orientation of the surface Fe and Co magnetization for the various alloy compositions. It is seen that the angle between the surface magnetization and the film plane decreases as the bulk Tb concentration decreases.

V. INFLUENCE OF THE MATERIAL PROPERTIES ON THERMOMAGNETICALLY WRITTEN DOMAINS

The relative independence of the width of the written domain on the applied (switching) field intensity in our films indicates that the formation of bits is dominated by nucleation processes and not by expansion or contraction of a single domain wall.[22] This is substantiated by the observation that for lower switching field strengths in iron-rich compositions, the written domains are not single domain but rather tiny magnetized regions oriented parallel and antiparallel to the field direction. This indicates that many indepen-

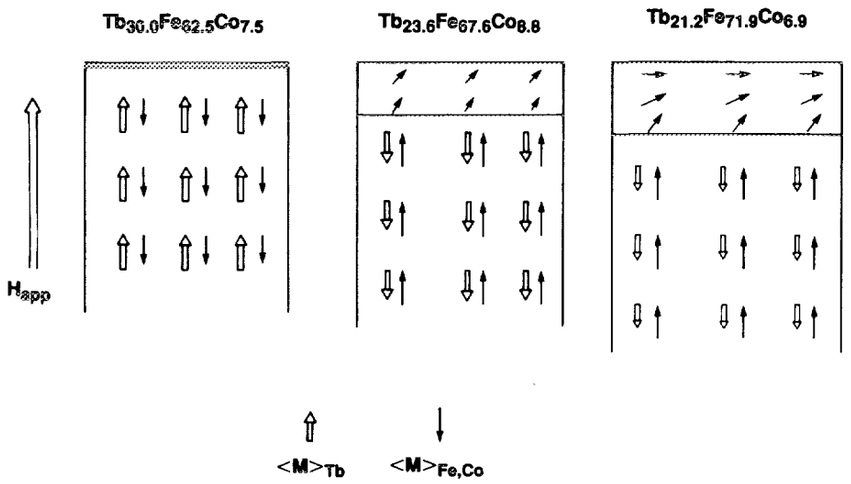

FIG. 7. Schematic cross section through the MO films. The hollow arrow indicates the direction of the Tb magnetic moment and the filled arrow is the direction of the Fe and Co magnetic moments. The external applied field direction is also shown.

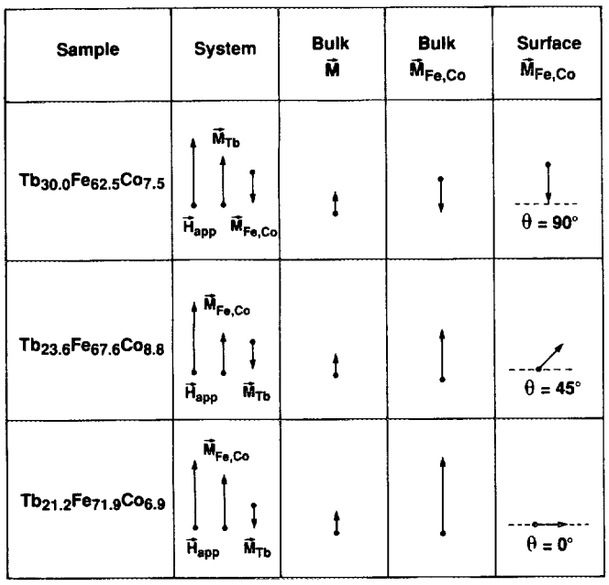

FIG. 8. Directions of the applied field, system, bulk, and surface magnetic moments for the constituents of the MO alloys as a function of alloy composition.

dent nucleation sites appear to be active. Therefore, wall movement as described by Hansen by a "bubble-type" model[13] was not observed, even in sample 2 (27.2% Tb), where the compensation temperature is near room temperature.

Among the magnetic parameters which effect the growth and nucleation of domains, T_{comp} plays a special role because its value drastically effects the temperature dependence of the saturation magnetization M_s and the coercive field H_c, as illustrated in Figs. 1 and 2. Tanaka, Tanaka, and Imamura[23] published carrier-to-noise (C/N) studies obtained by the MFM method using different sample compositions. They found that alloys with T_{comp} between room temperature and about 100 °C were suitable for MFM recording in MO media. Their conclusion is verified by comparing the TEM Lorentz and SEMPA images of sample 2 (27.2% Tb, $T_{comp} = 37$ °C) with the images from the other samples which have T_{comp} outside of Tanaka's temperature range. At lower Tb concentrations, i.e., samples 3 (23.6% Tb) and 4 (21.2% Tb), at all but the highest switching field intensities, the bits tend to break into a fine maze of upward and downward oriented subdomains. For very low switching fields (0 and 80 Oe), we observe no crescent-shaped domains. This undesirable configuration results from the lowering of the system demagnetizing energy. As cooling occurs in the thermomagnetic writing process, the region of reversed magnetization inside the initial domain wall increases as does the negative contribution to the demagnetizing field inside the still hot domain center. If this negative contribution to the demagnetizing field from the region of reversed magnetization, which has just nucleated, is large enough, it will dominate the nucleation field. Thus, it will cause demagnetization inside the written bit by inversely magnetized subdomain formation [see, e.g., Fig. 6(d)].[22]

The regularity of the written domains also depends upon the direction of the background magnetization in the film window. Observation of written bits in the fourth column from the left in Figs. 4(h) and 4(k) show that subdomain formation within each thermomagnetically written domain occurs preferentially in those bits aligned with the background magnetization. This feature can also be very well seen in the magnitude images in Figs. 4(i) and 4(l). The magnitude of the magnetization for bits oriented parallel to the background magnetization is less than that for bits oriented antiparallel to the background magnetization due to small inversely magnetized subdomain formation (smaller than the probe radius). This asymmetric switching behavior can be explained by taking into account the demagnetizing field arising from the neighboring region of the "background." The demagnetizing field from the "white" background points into the plane, and thus a larger switching field strength is needed to switch the bits from black to white, than from white to black. A small dc magnetic field oriented parallel to the background magnetization may help reduce this effect. Sample 2 (27.2% Tb) has the lowest saturation field, i.e., that field at which black and white written bits are completely switched. Since T_{comp} is slightly above room temperature for sample 2, the net magnetization of the unheated background is nearly zero and thus the background causes no asymmetric contribution to the demagnetizing field within the heated area.

For Tb-rich samples such as sample 1 (30% Tb) with T_{comp} above T_c, the coercive field rises steeply below the Curie temperature (Fig. 1), whereas the saturation magnetization rises more slowly (Fig. 2). Therefore, the low demagnetizing field makes nucleation difficult resulting in dendritic growth around nucleation centers frozen in before complete switching could occur.[7] The raggedness of the domain walls can be attributed to a local variation of the wall coercivity.[24] As the applied field gets higher, the domain walls become smoother because the local coercivity variation becomes less important.

The contrast between the domain nucleation process in the Tb-rich and transition-metal-rich alloys, as evidenced by the domain images in Figs. 3 and 4, suggest for TbFeCo alloys that the demagnetizing field is the most important parameter for domain regularity, in agreement with the conclusion of Tanaka *et al.*[23] We emphasize that the relevant demagnetizing field is the field at the temperature and region where nucleation is possible. To achieve good domain regularity for thermomagnetically written bits, the induced demagnetizing field should not be too low to make nucleation difficult, as in sample 1 (30% Tb), and the demagnetizing field should not be too high to enable reversed *sub*domain formation, as in samples 3 (23.5% Tb) and 4 (21.2% Tb).

VI. CONCLUSION

The magnetic microstructure of thin TbFeCo-alloy magneto-optic films has been investigated with both TEM Lorentz and SEMPA. SEMPA contrast is dominated by the $3d$ valence electrons from the transition metals in these ferrimagnetic alloys. The domain structure observed with these two techniques is similar even with the extremely complicated surface magnetic microstructure present in these films. A

simple model for surface segregation and oxidation of the rare-earth component of the alloy was sufficient to explain qualitatively the variation in the observed surface magnetic microstructure. Nucleation and switching of domains was found to be dominated by the demagnetizing fields for all but the highest Tb concentration alloys. The role of the surface segregation layer on the switching behavior in these materials is a topic for further investigation.

ACKNOWLEDGMENTS

This work was supported in part by the Office of Naval Research and by the Schweizerische Nationalfonds. We wish to thank B. A. J. Jacobs and J. H. M. Spruit for their contributions to the recording experiments, M. Rosenkranz for preparing the samples, M. H. Kelley for developing the image processing software, and D. T. Pierce and R. J. Celotta for stimulating discussions.

[1] H-P. D. Shieh and M. H. Kryder, Appl. Phys. Lett. **49,** 473 (1986).
[2] Y. Suzuki, N. Ohta, M. Takahashi, and S. Yonezawa, Appl. Phys. Lett. **55,** 315 (1989).
[3] M. Hartmann, B. A. J. Jacobs, and J. J. Braat, Philips Tech. Rev. **42,** 37 (1985).
[4] F. Tanaka, S. Tanaka, and S. Suzuki, IEEE Trans. Magn. **MAG-23,** 2695 (1987).
[5] D. Rugar, C. J. Lin, and R. H. Geiss, IEEE Trans. Magn. **MAG-23,** 2263 (1987).
[6] C. J. Lin, J. C. Suit, and R. H. Geiss, J. Appl. Phys. **63,** 3835 (1988).
[7] F. J. A. M. Greidanus, B. A. J. Jacobs, J. H. M. Spruit, and S. Klahn, IEEE Trans. Magn. **MAG-25,** 3524 (1989).
[8] J. W. Jacobs and J. F. Verhoeven, J. Microsc. **143,** 103 (1986).
[9] J. Unguris, G. Hembree, R. J. Celotta, and D. T. Pierce, J. Magn. Magn. Mater. **54–57,** 1629 (1986).
[10] D. R. Penn, Phys. Rev. B **35,** 482 (1987).
[11] M. P. Seah and W. A. Dench, Surf. Interf. Anal. **1,** 2 (1979).
[12] P. C. D. Hobbs, D. W. Abraham, and H. K. Wickramanasinghe, Appl. Phys. Lett. **55,** 2357 (1989).
[13] P. Hansen, J. Appl. Phys. **62,** 216 (1987).
[14] H. Miyajima, K. Sato, and T. Mizoguchi, J. Appl. Phys. **47,** 4669 (1976).
[15] J. J. M. Ruigrok, F. J. A. M. Greidanus, W. F. Godlieb, and J. H. M. Spruit, J. Appl. Phys. **63,** 3847 (1988).
[16] F. J. A. M. Greidanus, B. A. J. Jacobs, F. J. A. den Broeder, J. H. M. Spruit, and M. Rosenkranz, J. Appl. Phys. **66,** 4917 (1989).
[17] M. R. Scheinfein, J. Unguris, M. H. Kelley, D. T. Pierce, and R. J. Celotta, Rev. Sci. Instrum. **61,** 2501 (1990).
[18] P. Bernstein and C. Gueugnon, J. Appl. Phys. **55,** 1760 (1984).
[19] S. Klahn, H. Heitmann, M. Rosenkranz, and H. J. Tolle, J. Phys. (Paris) Colloq. **49,** C8-1711 (1989).
[20] M. Aeschlimann, G. L. Bona, F. Meier, M. Stampanoni, A. Vaterlaus, H. C. Siegmann, E. E. Marinero, and H. Notarys, IEEE Trans. Magn. **MAG-24,** 3180 (1988).
[21] M. Aeschlimann, G. L. Bona, F. Meier, M. Stampanoni, A. Vaterlaus, and H. C. Siegmann, Proceedings of the Symposium on Magnetic Properties of Amorphous Metals, Benalmadena, Spain, May 1987, p. 70.
[22] J. C. Suits, D. Rugar, and C. J. Lin, J. Appl. Phys. **64,** 252 (1988).
[23] F. Tanaka, S. Tanaka, and N. Imamura, Jpn. J. Appl. Phys. **26,** 231 (1987).
[24] C. J. Lin and D. Rugar, IEEE Trans. Magn. **MAG-24,** 2311 (1988).